Ionization and electron capture in collisions of bare carbon ions with hydrogen

I. B. Abdurakhmanov, K. Massen-Hane, Sh. U. Alladustov, J. J. Bailey, A. S. Kadyrov, and I. Bray

Phys. Rev. A **98**, 062710 — Published 19 December 2018

DOI: 10.1103/PhysRevA.98.062710

Ionization and electron capture in collisions of bare carbon ions with hydrogen

I. B. Abdurakhmanov, K. Massen-Hane, Sh. U. Alladustov, J. J. Bailey, A. S. Kadyrov, and I. Bray
Curtin Institute for Computation and Department of Physics and Astronomy,
Curtin University, GPO Box U1987, Perth, WA 6845, Australia
(Dated: November 19, 2018)

Ionization and electron capture in collisions of bare carbon ions with atomic hydrogen has been studied using the wavepacket continuum discretization approach. The three-body Schrödinger equation governing the collision process is solved using the two-center expansion of the total scattering wavefunction. Calculations have been performed for the projectile energy range from 1 keV/amu to 10 MeV/amu. While there is excellent agreement with experimental data for the total electron-capture cross section over the entire energy range, the calculated total ionization cross section slightly overestimates the only available measured point. The singly and doubly differential ionization cross sections at 1 and 2.5 MeV/amu are in good agreement with experiment. The differential cross section calculations are extended to lower energies where perturbative methods are expected to fail. At 100 keV/amu impact energy the present singly differential cross section in the ejected angle of the electron shows a pronounced peak in the forward direction. It is concluded that at low incident energies electron capture into the continuum of the projectile strongly enhances electron ejection in the forward direction.

PACS numbers: 34.10.+x, 34.50.Bw

I. INTRODUCTION

Collisions of bare carbon ions with atomic hydrogen is a three-body scattering problem where the target electron is exposed to the strongly asymmetric two-center Coulomb field. Due to the long-range attraction of the projectile the multiple scattering effects are important on a wide energy range making the first-order approaches problematic even at considerably high impact energies. Apart from fundamental interest this collision system is also of considerable importance in practical applications such as plasma modeling [1]. For instance, in the ITER project, the proposed neutral hydrogen beam heating of the magnetically confined plasma can initiate collisions between atomic hydrogen and various impurity ions. Furthermore, methods such as charge-exchange recombination spectroscopy, beam emission spectroscopy, and motional Stark effect spectroscopy, can provide information about field strength, temperature, density, and magnetic field orientation. These diagnostic methods require accurate data on charge-transfer, ionization and excitation cross sections [2]. Considering that the first-order theories do not perform very well for moderately energetic highly-charged projectiles, more sophisticated non-perturbative approaches need to be used for calculations on the entire energy range of interest.

Another practical application is *hadron therapy of cancer*, where beams of protons and bare carbon ions are used to eliminate tumor cells [3]. The carbon projectiles are considered to be more efficient as their Bragg peak in the radiation dose distribution curve is significantly sharper which reduces the amount of the radiation delivered to surrounding normal tissue. Accurate cross section data for collisions of carbon projectiles with relevant targets can potentially improve treatment outcomes. Testing the theoretical model on the simplest target is therefore a necessary first step.

Experimental studies of $C^{6+}-H$ collisions are very limited due to the difficulties associated with obtaining a sufficiently intense beam of fully-stripped carbon ions. For the total electron-capture cross section the data are available at low (1–10 keV/amu) [4] and intermediate (100-200 keV/amu) [5] energy regions. The total ionization cross section was measured only at 400 keV/amu by Shah and Gilbody [6]. The measurements of singly and doubly differential cross sections of ionization as a function of the ejected electron's energy and angle were performed at 1 and 2.5 MeV/amu impact energies by Tribedi et al. [7, 8, 9].

From a theoretical point of view there exists quite extensive research on C^{6+}-H collisions. The earliest works were based on the first Born approximation (FBA) which neglects multiple-scattering effects and coupling between reaction channels. Excitation, electron-capture and ionization channels are all considered separately. Investigations of the electron-capture process in $C^{6+}-H$ collisions go back to the pioneering works of Oppenheimer [10] and Brinkman and Kramers [11] who neglected the internuclear potential. Later, Jackson and Schiff [12] demonstrated the importance of this potential even for highest impact energies where the FBA was expected to be reliable. However, the electron-capture cross sections obtained by Jackson and Schiff [12] still overestimated the measured data of Goffe et al. [5] by an order of magnitude. Further investigations revealed that at high energies the FBA is valid only for the description of ionization, while an adequate treatment of electron capture requires inclusion of at least the second order term in the perturbation. This is due to the fact that the electron-capture process in energetic collisions involves multiple scattering mechanism [13]. For this reason, the FBA type approaches, even the ones which include the inter-

action potentials between all reaction constituents, fail to describe the electron-capture process at high impact energies.

Belkic et al. [14] stated that the large discrepancy with the experiment for the electron-capture cross section was caused by the inadequacy of the FBA approach of Jackson and Schiff [12] to account for the long-range Coulomb interaction between the target proton and the traveling C^{5+} ion formed after capturing the electron. To address this problem Belkic et al. [14] developed a so-called boundary-corrected first Born approximation abbreviated as B1B. They introduced a Coulomb distortion in the form of a logarithmic phase factor to modify the outgoing wave in the exit channel. The B1B results of Belkic et al. [14] agree well with the measured data of Goffe et al. [5].

The continuum-distorted-wave (CDW) method also takes into account multiple scattering effects. The method and its applications to electron-capture problems were reviewed by Belkic et al. [15]. Crothers and McCain [16] and Rivarola et al. [17] developed a continuum-distorted-wave eikonal-initial-state (CDW-EIS) approach and applied to ionization.

The classical-trajectory Monte Carlo (CTMC) technique was utilized by several authors [18–23] to calculate ionization and electron capture processes in C^{6+}-H collisions. The computational cost of this approach is relatively low. However, the reliability of the results depends on the quality of the underlying statistics; therefore, the method requires a very large number of trajectory calculations to be carried out.

The aforementioned approaches to the problem are all perturbative methods without coupling between various possible reaction channels. Each channel is considered as independent. The most reliable methods in scattering theory, which allow calculating elastic scattering, excitation, ionization and electron-capture cross sections in state resolved levels, are based on the lattice and the two-center atomic and molecular-orbital close-coupling approaches. The first approach solves the semiclassical time-dependent Schrödinger equation for the electronic scattering wave function directly by discretizing the space coordinates. The accuracy of the final results in this method is ensured by choosing a sufficiently large and densely-discretized space grid. However, the method quickly becomes impractical and overly time-consuming for collisions with highly charged projectiles, since much larger space needs to be discretized as the projectile charge increases. The molecular-orbital close-coupling (MOCC) approach [24–26] treats the collision system as a molecule. The method is reliable and practical at a near-adiabatic regime where the incident energy of the projectile is sufficiently low. The atomic-orbital close-coupling (AOCC) approach [22, 27, 28] solves the semiclassical time-dependent Schrödinger equation by expanding the scattering wave function in terms of a linear combination of traveling atomic orbitals localized on the two nuclear centers. The main challenge of the AOCC approaches is to achieve convergence of the final results with respect to the number of target and projectile states before running into issues with ill-conditioned systems which can occur as a result of overly large expansions and inaccuracies in the interaction matrix elements. For highly-charged projectiles achieving convergence is even more complicated as the target electron can be captured to projectile states with large principal quantum numbers. The collision data obtained by the AOCC approach are available at low to intermediate energies [22, 27, 28]. At higher energies where the cross section for the ionization channel should merge with the results of FBA the AOCC calculations become time-consuming since in this kinematic regime the integrands of the rearrangement matrix elements required to describe electron capture process are extremely oscillatory. For this reason no AOCC results for C^{6+}-H collisions have been available so far at energies higher than 500 keV/amu.

In this work we consider scattering of bare carbon ions on atomic hydrogen on a wide projectile energy range from 1 keV/amu to 10 MeV/amu using one unified approach and make a comparison of the obtained results with the published results of the MOCC, AOCC, CTMC, CDW-EIS, B1B and FBA approaches which perform well in various parts of the considered energy range. To this end our two-center semiclassical wavepacket convergent close-coupling (WP-CCC) approach [29] to proton-hydrogen collisions is extended to take arbitrary charges and masses for the nuclei of the collision system. However, one must note that in these heavy particle collisions, the masses of the proton and carbon nucleus can be taken as infinite compared to that of the electron. The full three-body Schrödinger equation is solved by expanding the total scattering wave function in a two-center basis of atomic wave functions. This leads to a set of coupled differential equations for the transition probability amplitudes which are used to calculate the cross sections for elastic scattering, target excitation, electron capture by the projectile and ionization. The wave functions representing atomic hydrogen are the true eigenfunctions for the negative-energy states and orthonormal stationary wave packets for positive-energy states. The wave packets representing the target continuum are constructed using the Coulomb wave function, the eigenstate of the hydrogenic Hamiltonian. The basis functions on the projectile center representing the states of the C^{5+} ion are obtained in a similar way taking into account the charge and mass of the nucleus. Convergence of state-resolved and total cross sections is achieved by increasing the number of included negative-energy eigenstates and positive-energy pseudostates for the projectile-electron and target-electron systems. In addition to introducing arbitrary nuclear charges, the underlying computer code has also been enhanced with OpenACC features [30] which offload most of the computation to the graphical processing units (GPU). This gives up to a two orders of magnitude speedup over the original computer code that runs on traditional central processing units. This up-

grade allows us to include a considerably larger number of atomic orbitals as well as to increase the accuracy of calculations in kinematic regimes which have been problematic for previous two-center AOCC approaches.

The paper is set out as follows. In Sect. II we give a brief outline of the formalism. The results of calculations are presented in Sect. III. Finally in Sect. IV we highlight the principal findings and draw conclusions. Unless specified otherwise, atomic units are used throughout.

II. FORMALISM

The basic formalism of the wavepacket convergent close-coupling approach to proton-hydrogen collisions is given in [29, 31]. It has been extended to two-electron targets in [32]. In this paper we generalize this approach to the collisions of bare ions with hydrogenic targets consisting of a nucleus and one electron. This type of collisions represents a three-body Coulomb scattering problem. Therefore, the required modifications to the existing WP-CCC approach are minimal and involve only allowing for arbitrary charge and mass of the two nuclei. Scattering of a projectile with charge Z_p off the one-electron target with nucleus charge Z_t is governed by the following full three-body Schrödinger equation for the total scattering wave function with the outgoing-wave boundary conditions:

$$(H-E)\Psi_i^+ = 0, \tag{1}$$

where E is the total energy and H is the full three-body Hamiltonian of the collision system. Index i denotes the initial channel, from which the total scattering wave develops. In the present work it is taken to be the projectile of energy E_in incident on H in the ground state. The equation (1) is solved by expanding the total scattering wave function in terms of the target (ψ_α) and projectile (ψ_β) pseudostates as

$$\Psi_i^+ \approx \sum_{\alpha=1}^{N} F_\alpha(t,\boldsymbol{b})\psi_\alpha(\boldsymbol{r}_\mathrm{t})e^{i\boldsymbol{q}_\alpha\cdot\boldsymbol{\rho}} + \sum_{\beta=1}^{M} G_\beta(t,\boldsymbol{b})\psi_\beta(\boldsymbol{r}_\mathrm{p})e^{i\boldsymbol{q}_\beta\cdot\boldsymbol{\sigma}}, \tag{2}$$

where F_α and G_β are time-dependent coefficients, and N and M are the numbers of basis functions on the target and projectile centers. Eq. (2) is written in terms of the variables of the Jacobi coordinates, where index α denotes a quantum state in a channel where projectile of relative momentum $\boldsymbol{q}_\alpha$ is incident on a bound state of the target atom. Index β denotes a quantum state in the rearrangement channel, where the atom formed by the projectile after electron capture has momentum $\boldsymbol{q}_\beta$ relative to the stripped target nucleus. The position of the projectile with respect to the centre of mass of the target nucleus-electron pair is denoted by $\boldsymbol{\rho}$, while $\boldsymbol{\sigma}$ is the position of the projectile-electron pair with respect to the target nucleus. $\boldsymbol{R}$ represents the position vector of the projectile relative to the target nucleus. In this work we assume that the target nucleus is located at a fixed origin and the projectile is moving along a straight-line classical trajectory $\boldsymbol{R} = \boldsymbol{b} + \boldsymbol{v}t$, where $\boldsymbol{b}$ is the impact parameter and $\boldsymbol{v}$ is the projectile velocity. The impact parameter is defined so that $\boldsymbol{b}\cdot\boldsymbol{v} = 0$. The position of the electron relative to the target proton is $\boldsymbol{r}_\mathrm{t}$, while $\boldsymbol{r}_\mathrm{p}$ is the electron position relative to the projectile. The sets of projectile (C^{5+}) and target (H) pseudostates are constructed from the combination of negative-energy eigenstates and positive-energy wavepacket pseudostates in a similar way as described in [29], but taking into account the charge of the corresponding nucleus. The wavepacket pseudostates form an orthonormal set of basis functions separately for the target and projectiles atoms. However, the pseudostates from one set are not orthogonal to the pseudostates from another set. In addition, the wavepacket pseudostates from the target-centered set diagonalize the Hamiltonian of atomic hydrogen and the ones from the projectile-centered set diagonalize the Hamiltonian of the C^{5+} atom formed by the incident C^{6+} after capturing the electron.

With this expansion and a semiclassical approximation the Schrödinger equation (1) can be transformed to the set of first-order differential equations for the time-dependent coefficients

$$\begin{cases} i\dot{F}_{\alpha'} + i\sum_{\beta=1}^{M}\dot{G}_\beta\tilde{K}_{\alpha'\beta} = \sum_{\alpha=1}^{N}F_\alpha D_{\alpha'\alpha} + \sum_{\beta=1}^{M}G_\beta\tilde{Q}_{\alpha'\beta}, \\ i\sum_{\alpha=1}^{N}\dot{F}_\alpha K_{\beta'\alpha} + i\dot{G}_{\beta'} = \sum_{\alpha=1}^{N}F_\alpha Q_{\beta'\alpha} + \sum_{\beta=1}^{M}G_\beta\tilde{D}_{\beta'\beta}, \\ \alpha' = 1,2,\ldots,N, \quad \beta' = 1,2,\ldots,M, \end{cases} \tag{3}$$

where dots over F_α and F_β denote time derivatives. Here overlap integrals are given as

$$K_{\beta'\alpha}(\boldsymbol{R}) = \langle\psi_{\beta'}|\exp\left[-i\boldsymbol{v}\cdot\boldsymbol{r}_\mathrm{t}\right]|\psi_\alpha\rangle \times \exp\left[iv^2t/2 + i(\varepsilon_{\beta'}-\varepsilon_\alpha)t\right], \tag{4}$$

$$\tilde{K}_{\alpha'\beta}(\boldsymbol{R}) = \langle\psi_{\alpha'}|\exp\left[i\boldsymbol{v}\cdot\boldsymbol{r}_\mathrm{t}\right]|\psi_\beta\rangle \times \exp\left[-iv^2t/2 + i(\varepsilon_{\alpha'}-\varepsilon_\beta)t\right], \tag{5}$$

where ε_α (ε_β) is the energy of the target (projectile) state. Direct-scattering matrix elements are given as

$$D_{\alpha'\alpha}(\boldsymbol{R}) = \langle\psi_{\alpha'}|\overline{V}_\alpha|\psi_\alpha\rangle\exp\left[i(\varepsilon_{\alpha'}-\varepsilon_\alpha)t\right], \tag{6}$$

$$\tilde{D}_{\beta'\beta}(\boldsymbol{R}) = \langle\psi_{\beta'}|\overline{V}_\beta|\psi_\beta\rangle\exp\left[i(\varepsilon_{\beta'}-\varepsilon_\beta)t\right], \tag{7}$$

where $\overline{V}_\alpha = Z_\mathrm{t}Z_\mathrm{p}/R - Z_\mathrm{p}/r_\mathrm{p}$ and $\overline{V}_\beta = Z_\mathrm{t}Z_\mathrm{p}/R - Z_\mathrm{t}/r_\mathrm{t}$. Electron-transfer matrix elements are given as

$$Q_{\beta'\alpha}(\boldsymbol{R}) = \langle\psi_{\beta'}|\exp\left[-i\boldsymbol{v}\cdot\boldsymbol{r}_\alpha\right](H_\alpha + \overline{V}_\alpha - \varepsilon_\alpha)|\psi_\alpha\rangle \times \exp\left[iv^2t/2 + i(\varepsilon_{\beta'}-\varepsilon_\alpha)t\right], \tag{8}$$

$$\tilde{Q}_{\alpha'\beta}(\boldsymbol{R}) = \langle\psi_{\alpha'}|\exp\left[i\boldsymbol{v}\cdot\boldsymbol{r}_\alpha\right](H_\beta + \overline{V}_\beta - \varepsilon_\beta)|\psi_\beta\rangle \times \exp\left[-iv^2t/2 + i(\varepsilon_{\alpha'}-\varepsilon_\beta)t\right], \tag{9}$$

where H_α and H_β are the target and projectile atom Hamiltonians. We emphasize that Eqs. (3)-(9) coincide with the correspondng equations resulting from the conventional semiclassical approach when plane-wave electron translation factors are introduced [33]. For further details of the derivation, see Ref. [29].

The expansion coefficients $F_\alpha(t,\boldsymbol{b})$ and $G_\beta(t,\boldsymbol{b})$ at $t\to\infty$ represent the transition amplitudes (in the impact-parameter representation) into the target and projectile pseudostates and at $t\to-\infty$ satisfy the initial boundary condition

$$\begin{cases} F_\alpha(-\infty,\boldsymbol{b}) = \delta_{\alpha 1}, & \alpha = 1,2,\ldots,N, \\ G_\beta(-\infty,\boldsymbol{b}) = 0, & \beta = 1,2,\ldots,M. \end{cases} \tag{10}$$

The direct-scattering matrix elements are calculated in the spherical coordinates, while the overlap integrals and the electron-transfer matrix elements are evaluated using the spheroidal coordinates as described in [34]. The existing computational code which solves Eq. (3) has been modified to run on GPU based supercomputers which reduced the computational time by orders of magnitude. Offloading computation of the direct, overlap and electron-transfer matrix elements to GPUs is achieved through utilization of the OpenACC directives recently introduced to Fortran [30], while the CUDA library, *cuSolverDn* [35], is used to solve the system of linear equations emerging at each time step of the Runge-Kutta propagation.

Once the expansion coefficients $F_\alpha(t,\boldsymbol{b})$ and $G_\beta(t,\boldsymbol{b})$ are found at $t\to\infty$ the integrated and differential cross sections for all included electronic transitions can be calculated using the technique given in Ref. [29].

The present WP-CCC approach also allows to calculate all types of differential ionization cross sections including the fully differential one. This can be realized due to the feature of the wave-packet bin states describing the continuum. Once the time-dependent coefficients in Eq. (3) are found the two-center scattering wave function can be reconstructed using Eq. (2). The most detailed ionization amplitude which is used to calculate the fully, five-fold differential cross section can be found by projecting the Coulomb wave describing the final ionized state of the electron onto the two-center scattering wave function. Since the wave-packet bin states themselves are constructed from the Coulomb wave function this procedure becomes much simpler. Full details of the WP-CCC approach to differential ionization is given in [29]. Here, we only give the final expression for the fully differential cross section. In the current two-center WP-CCC approach it consists of incoherent combination of two components, namely direct ionization (DI) and electron-capture into continuum (ECC) [37]:

$$\frac{d^3\sigma_{\rm ion}(\boldsymbol{\kappa},\boldsymbol{q}_f,\boldsymbol{q}_i)}{dE_{\rm e}d\Omega_{\boldsymbol{\kappa}}d\Omega_{\boldsymbol{q}_f}} = \mu^2\frac{q_f\kappa}{q_i}\Big(\big|T_{fi}^{\rm DI}(\boldsymbol{\kappa},\boldsymbol{q}_f,\boldsymbol{q}_i)\big|^2 + \big|T_{fi}^{\rm ECC}(\boldsymbol{\kappa}-\boldsymbol{v},\boldsymbol{q}_f,\boldsymbol{q}_i)\big|^2\Big), \tag{11}$$

where μ is the reduced mass of the collision system, and $\boldsymbol{q}_i$ and $\boldsymbol{q}_f$ are the projectile momentum before and after collision, respectively. The ionization amplitudes $T_{fi}^{\rm DI}(\boldsymbol{\kappa},\boldsymbol{q}_f,\boldsymbol{q}_i)$ and $T_{fi}^{\rm ECC}(\boldsymbol{\kappa}-\boldsymbol{v},\boldsymbol{q}_f,\boldsymbol{q}_i)$ are directly related to the time-dependent coefficients $F_\alpha(t,\boldsymbol{b})$ and $F_\beta(t,\boldsymbol{b})$ at asymptotic region $t\to\infty$, respectively. In the single-center WP-CCC approach $T_{fi}^{\rm ECC}(\boldsymbol{\kappa}-\boldsymbol{v},\boldsymbol{q}_f,\boldsymbol{q}_i)=0$. A cross section differential in a particular variable is obtained by integrating the fully differential cross section over all other variables.

III. RESULTS AND DISCUSSION

In all atomic orbital close-coupling approaches, including this work, the quality of the final results depends on several factors, such as the size of the employed target and projectile bases, the type of orbitals representing the bound and continuum states of the electron and the accuracy of the matrix elements appearing in the scattering equations. Since in C^{6+}-H scattering the target electron is exposed to the largely asymmetric two-center Coulomb field, the accuracy of cross sections for various processes taking place in the system may have a different sensitivity to the numbers of bound and continuum states of atomic hydrogen and C^{5+} ion used to construct the total two-center scattering wave function describing the problem. For instance, the accuracy of the electron-capture cross sections mostly depend on the number of included bound states of the C^{5+} ion. Since the ground-state energy of the C^{5+} ion is $Z_\alpha^2=36$ times lower than the ground-state energy of atomic hydrogen it is logical to think that the inclusion of more C^{5+} bound states than hydrogen bound states is required. At the same time, the total ionization cross section consists of two parts, one corresponding to direct ionization of the target and the other to electron capture into the continuum of the projectile. Therefore, it is expected to be sensitive to the number of included positive-energy pseudostates (hereafter called simply continuum states) on both target and projectile. The relative contribution of the target and projectile continua is energy dependent. Therefore, rather than attempting to choose the optimal asymmetric two-center basis, in this work, we utilize the same number of bound and continuum states of atomic hydrogen and C^{5+} ion and pay careful attention to the convergence of the cross sections for each of the occurring processes. Though this approach might not be optimal for all impact energies, it is much simpler and with the GPU based acceleration is readily achievable.

Accurate final results can be obtained by examining their convergence with respect to the parameters characterizing the motion of the projectile and the structure of the target and the projectile-electron system, such as the maximum included orbital angular momentum quantum number $l_{\rm max}$, the number of bound (negative-energy) eigenstates $N_{\rm b}-l$, the maximum energy $\varepsilon_{\rm max}(=\kappa_{\rm max}^2/2)$ of the electron continuum covered by the wavepacket

bins, and the number of bins within this interval N_c. The optimal maximum energy ε_{max} can be chosen by analyzing the behaviour of the singly differential cross section (SDCS) in the ejected electron energy. For instance, in Fig. 1 we show the contributions to the SDCS from direct ionization (DI) and electron capture into continuum (ECC) as functions of the ejected electron energy at the impact energies of 400 keV/amu and 1 MeV/amu. One can see that $\varepsilon_{max} = 350$ eV for the incident energy of 400 keV/amu and $\varepsilon_{max} = 1000$ eV for the incident energy of 1 MeV/amu is sufficiently large as the SDCS for higher ejected energies is more than three orders of magnitude smaller than the maximum, and therefore, can be neglected. One can note that the points in Fig. 1 indicate the positions of the wave-packet pseudostate energies. In this work we use a sufficiently dense parabolic grid for the distribution of the ejected electron energies and always ensure that the both DI and ECC components of the SDCS drop by at least three orders of magnitude in the ejected energy. Thus, inaccuracies associated with the neglected tail of the SDCS above ε_{max} does not exceed 0.1%. However, we must note that this is not the inaccuracy of the entire calculations. There are also inaccuracies associated with solving the system of coupled differential equations, linear dependency problems resulting from the extremely large two-center expansion basis, non-orthogonality between target and projectile basis functions at small internuclear distances, etc. Taking all of this into account, the overall numerical error of presented calculations is estimated to be less than 5%.

Also, by analyzing Fig. 1 one can observe that the contribution of the ECC component to the total ionization reduces as the incident projectile energy increases. This suggests the dominance of the DI channel at high impact energies. Note that the peak of the ECC component at around $\kappa = \sqrt{2\varepsilon} = v$ is more pronounced at 1 MeV/amu.

Having fixed the maximum value of the ejected electron energy we systematically increase the number of hydrogen and C^{5+} bound and continuum states per orbital angular symmetry until the desired level of convergence is achieved. In a similar way we establish convergence of the final results in terms of other parameters. The system of scattering equations (3) was solved using the standard Runge-Kutta method by varying the z-component of the projectile position from -150 to $+150$ a.u. at all incident energies. The accuracy of the solution is monitored by an adaptive approach where the lower and upper truncation error limits are set to be 10^{-6} and 10^{-4}, respectively. The unitarity is satisfied to three digits at all values of z.

We found the upper limit of the impact parameter, b_{max}, needs to be larger as the impact energy increases. At highest impact energy considered in this work $b_{max} =$ 70 a.u. was required to achieve an acceptable level of convergence of all considered cross sections. For lower impact energies the desirable convergence can be achieved with smaller values of b_{max}. Specifically, at the lowest considered incident energy $b_{max} = 20$ a.u. was sufficient. To perform accurate calculations we had to extend the radial grid of state orbitals up to 300 a.u.

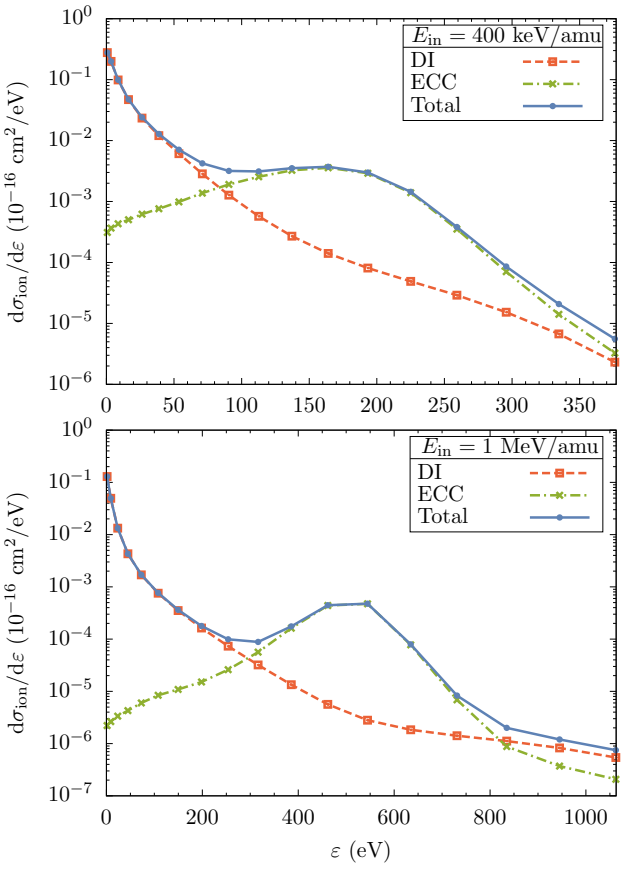

FIG. 1: (color online) The singly differential cross section, $d\sigma_{ion}/d\varepsilon$, for ionization in C^{6+}-H collisions as a function of energy of the ejected electron at 400 keV/amu and 1 MeV/amu impact energies. The separate contributions from direct ionization (DI) and electron capture into continuum (ECC) are also shown.

In his pioneering two-center coupled-state approach Bates [36] demonstrated that the effect of the internuclear term $Z_t Z_p/R$ on excitation, ionization and electron-capture channels can be consistently removed if the non-orthogonality of the target and projectile wave functions is properly accounted for. We used this fact to check the accuracy of the overlap matrix elements $K_{\beta'\alpha}(\boldsymbol{R})$ and $\tilde{K}_{\alpha'\beta}(\boldsymbol{R})$. Specifically, we have made calculations with and without internuclear term at 1, 10, 100 and 1000 keV/amu to verify that it has no effect on the aforementioned cross sections. Nevertheless we keep the internuclear term in our calculations to get complete information on the collision including the elastic cross section (not presented in this work but can be provided upon request).

A. Total electron-capture cross sections

The total cross section for electron capture in C^{6+}-H collisions is obtained from the sum of the partial cross sections for the transitions from the ground state of atomic hydrogen into all the included C^{5+} bound states. Therefore, this cross section is particularly sensitive to the number of bound eigenstates on the projectile center included in the expansion of the total scattering wave function. In Table I we show the convergence of the total electron-capture cross section with increasing number of bound eigenstates on the projectile and target centers, N_b, at three energy points, namely 1, 10 and 100 keV/amu. Other basis parameters are fixed at sufficiently large values. Specifically, $N_c = 20$ and $l_{max} = \min(N_b - 1, 6)$, whereas $\varepsilon_{max} = 400$ eV for impact energies ≤ 100 keV/amu and $\varepsilon_{max} = 1200$ eV for 1000 keV/amu.

TABLE I: Convergence of the total electron-capture cross section (10^{-16} cm^2) with respect to N_b at given incident energies. Notation: $A[-N]$ implies $A \times 10^{-N}$.

Energy (keV/amu)	$N_b = 5$	$N_b = 6$	$N_b = 8$	$N_b = 9$	$N_b = 10$
1	42.2	42.6	42.6	42.7	42.7
10	44.8	46.6	47.4	47.6	47.6
100	6.58	6.69	6.76	6.81	6.82
1000	6.03[-4]	6.04[-4]	6.04[-4]	6.04[-4]	6.04[-4]

Figure 2 presents the energy dependence of the total electron-capture cross section for C^{6+} collisions with the ground state of hydrogen at different values of the maximum allowed angular momentum of the target and projectile pseudostates. In the lower figure, results are given in the logarithmic scale to highlight the higher energy region. One can see a systematic convergence of the cross section with increasing l_{max}. Calculations with $l_{max} = 6$ produce very well converged results at all considered energies. It should also be noted that the results are already converged with angular momenta $l \leq 5$, since that is the range of angular momenta for the resonant state with $n = 6$. The rate of l-convergence is faster for higher impact energies and at energies above 1 MeV/amu the $l_{max} = 1$ results are reasonably well convergent.

In Fig. 3 the WP-CCC results are compared with the measurements of Meyer et al. [4] and Goffe et al. [5] and the results of other calculations. Generally, present results are in very good agreement with the experiment, the MOCC calculations of Harel et al. [24], the AOCC calculations of Igenbergs et al. [22] and the CTMC calculations of Jorge et al. [23] at all available energies. One should note the almost perfect agreement of the WP-CCC results with the AOCC results of Igenbergs et al. [22] at all considered energies (the visual discrepancy at 1-7 keV/amu energy range is due to the lack of calculated data by Igenbergs et al. [22]). It can be attributed to some similarities of the employed basis functions. Calculations of Igenbergs et al. [22] use all of the C^{5+} negative-energy eigenstates with $n \leq 11$, whereas the current approach uses the C^{5+} negative-energy eigenstates as well, however, with $n \leq 10$ and $l \leq 6$. The AOCC results of Toshima [27] with Gaussian-type basis functions are systematically lower in the energy range from 20 to 400 keV/amu. There are at least two possible reasons for the discrepancy. First, the AOCC calculations of Toshima [27] utilize considerably smaller number of bound C^{5+} states with $n \leq 6$ and $l \leq 5$. It means that no C^{5+} bound states were included in the region between -0.5 a.u. and 0. However, our calculations listed in Table I suggest that this should not be the reason for considerable discrepancy. Another possible reason might be the fact that the bound states of the C^{5+} ion used in calculations of Toshima [27] are not true eigenstates but the states constructed from the linear combination of Gauss-type basis functions. The energies of some of these states are slightly different from the corresponding exact values. The idea of Belkic et al. [14] to include the projectile induced distortion which fixes the boundary conditions in the FBA approximation resolved an order of magnitude discrepancy with the measurements of Goffe et al.

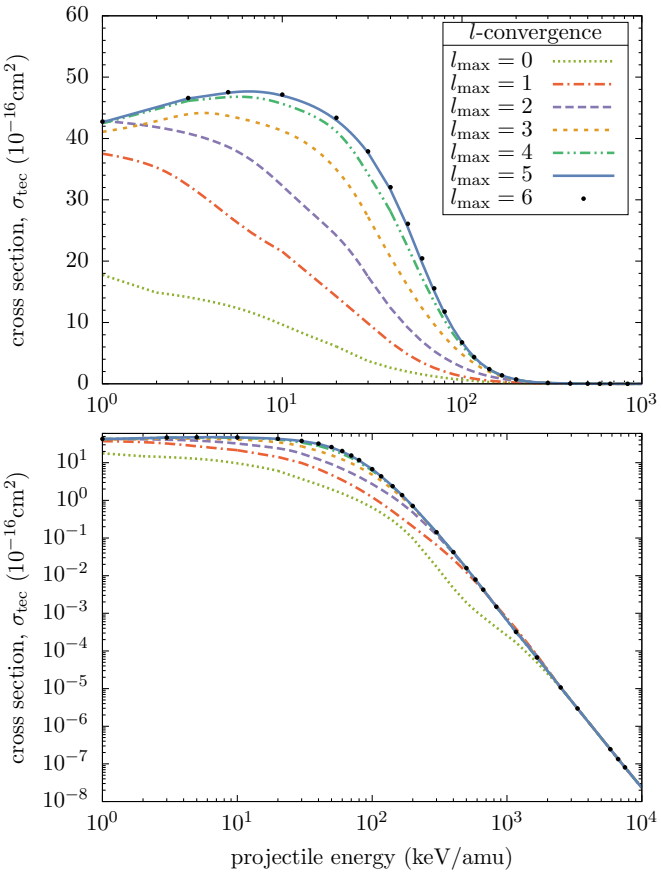

FIG. 2: (color online) The total cross section (σ_{tec}) for electron capture in C^{6+}-H($1s$) collisions: the convergence of the present WP-CCC results with respect to the maximum included orbital angular momentum quantum number l_{max}.

[5]. However, at energies below 100 keV/amu the results of Belkic et al. [14] are generally higher. One can see from the figure that for this collision system the FBA results for electron capture significantly overestimate the experiment and the results of the advanced theories at all energies. The results shown in the logarithmic scale show that this trend continues up to 10 MeV/amu. Thus, as far as the electron-capture cross section is concerned the FBA is not valid even at very high impact energies due to necessity to include higher order terms in the perturbation series.

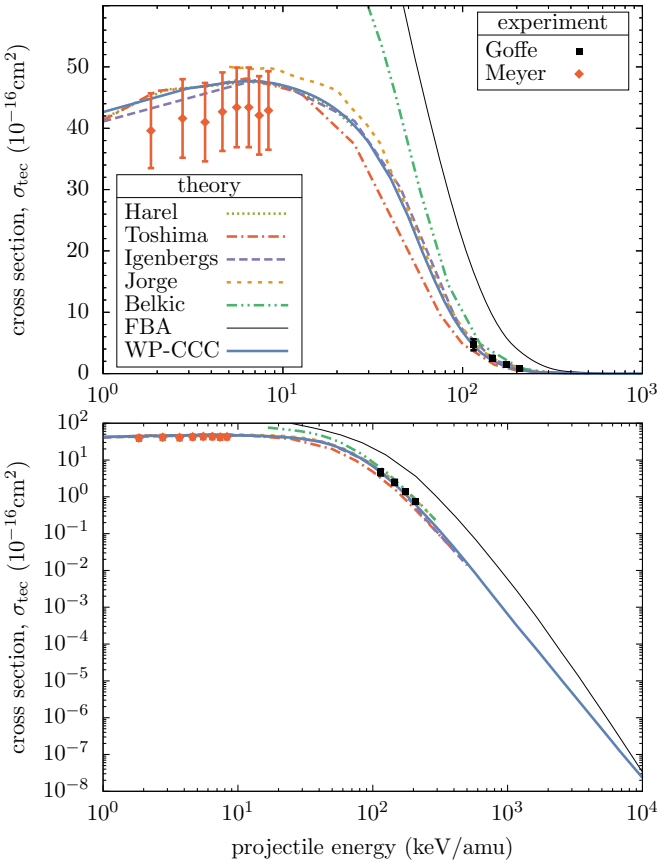

FIG. 3: (color online) The total cross section ($\sigma_{\rm tec}$) for electron capture in C^{6+}-H($1s$) collisions: the present WP-CCC results are compared with the experimental measurements of Goffe et al. [5] and Meyer et al. [4], and the MOCC calculations of Harel et al. [24], the AOCC calculations of Igenbergs et al. [22], Toshima [27], the CTMC calculations of Jorge et al. [23], the B1B calculations of Belkic et al. [14] with corrected boundary conditions, as well as the pure FBA results.

B. Total ionization cross sections

The total cross section for ionization in C^{6+}-H collisions is calculated as the sum of the partial cross sections for the transitions from the ground state of atomic hydrogen into all the included continuum states on the target and projectile centers. In Table II we show the convergence of the total ionization cross sections (TICS) with increasing number of continuum bin states on the projectile and target centers, $N_{\rm c}$, at three energy points, namely 50, 100 and 400 keV/amu. Other basis parameters are fixed at sufficiently large values, i.e.: $N_{\rm b} = 10$ (sufficient for the convergence of the total electron-capture cross section), $\varepsilon_{\rm max} = 400$ eV and $l_{\rm max} = 6$.

TABLE II: Convergence of the total ionization cross sections (10^{-16} cm^2) with respect to $N_{\rm c}$ at given incident energies.

Energy (keV/amu)	$N_{\rm c} = 10$	$N_{\rm c} = 18$	$N_{\rm c} = 19$	$N_{\rm c} = 20$
50	4.62	7.49	7.65	7.73
100	16.0	20.6	20.9	21.1
400	10.1	11.1	12.2	12.4

Figure 4 shows the energy dependence of the total cross section for the C^{6+}-impact ionization of atomic hydrogen with increasing $l_{\rm max}$. Again the lower figure shows the results in the logarithmic scale to highlight the higher energy region. The convergence pattern is not always monotonic with the cross section first increasing until $l_{\rm max} = 2$ and then decreasing to finally converge at $l_{\rm max} = 6$. Similar to the electron-capture cross sections, the rate of l-convergence of the total ionization cross sections is faster for higher impact energies.

Thus, the calculations, which yielded converged total ionization and electron-capture cross sections for all impact energies, employed a total of 2534 states (1267 on each center), where for each angular momentum $l \in [0:6]$ $N_{\rm b} = 10 - l$ bound states and $N_{\rm c} = 20$ continuum wavepacket pseudostates were used.

The present WP-CCC results are compared with the experiment [6] and other theories in Fig. 5. The current results overestimate the experiment by about 10%. This appears to be a common feature of all the coupled-channel approaches as they overestimate the experimental point roughly by a similar amount. Whether or not this is an artefact of the close-coupling formalism remains to be seen. The only exception is the CDW-EIS calculations of Rivarola et al. [17] which overlap with the lower limit of the experimental point.

Comparing the WP-CCC results with the results of other two AOCC calculations by Igenbergs et al. [22] and Toshima [27] one can see some variation at energies below 300 keV. This must be due to the differences in the two-center basis expansions used in these approaches. The approach of Toshima [27] with Gaussian-type functions is similar to the present approach in the sense that the continuum states are utilized on both projectile and target centers. However, as it was pointed out earlier the size of the Gaussian basis used in [27] was considerably smaller. The two-center AOCC approach of Igenbergs et al. [22] is different in the sense that they use continuum states only on the target center. Our experi-

ence with proton-hydrogen collisions [29, 34] showed that the approach where continuum states are included only on the target center does not produce convergent results showing a systematic increase with increasing l except at sufficiently high energies.

The CTMC results of Jorge et al. [23] are systematically higher than the present results, whereas the CDW-EIS results of Rivarola et al. [17] are significantly lower at all considered energies. At energies above 1 MeV/amu all presented theories agree with each other. Interesting to note that unlike the case for the electron-capture cross section, the WP-CCC results for ionization merge with the FBA results at a relatively lower impact energy, already above 2 MeV/amu. To be more specific, the WP-CCC results at 2.5 MeV/amu, 3.33 MeV/amu and 5.83 MeV/amu are 2.95×10^{-16}cm^2, 2.30×10^{-16}cm^2 and 1.41×10^{-16}cm^2, respectively, whereas the FBA results at these energies are 3.11×10^{-16}cm^2, 2.40×10^{-16}cm^2 and 1.46×10^{-16}cm^2.

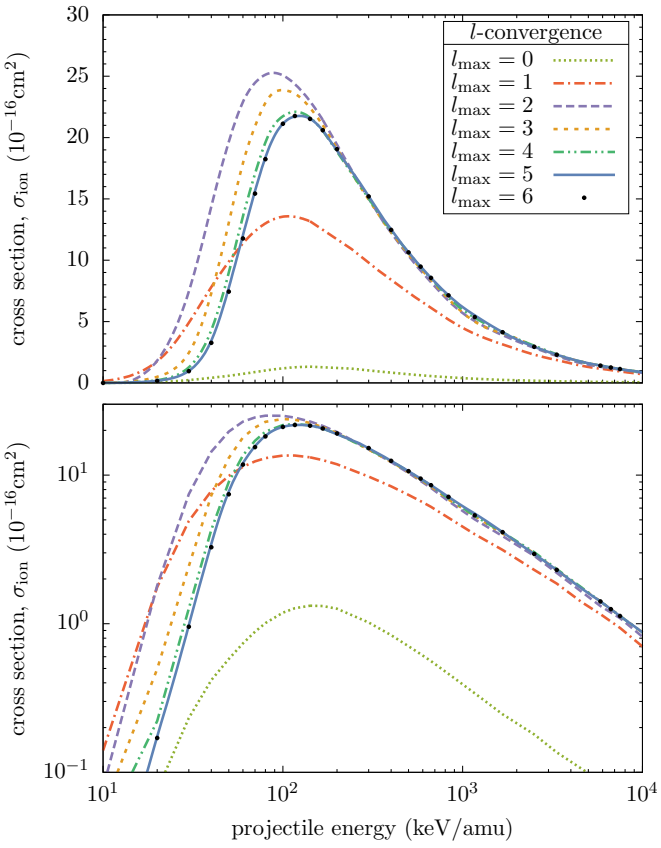

FIG. 4: (color online) The total cross section ($\sigma_{\rm ion}$) for ionization in C^{6+}-H($1s$) collisions: the convergence of the present WP-CCC results with respect to the maximum included orbital angular momentum quantum number $l_{\rm max}$.

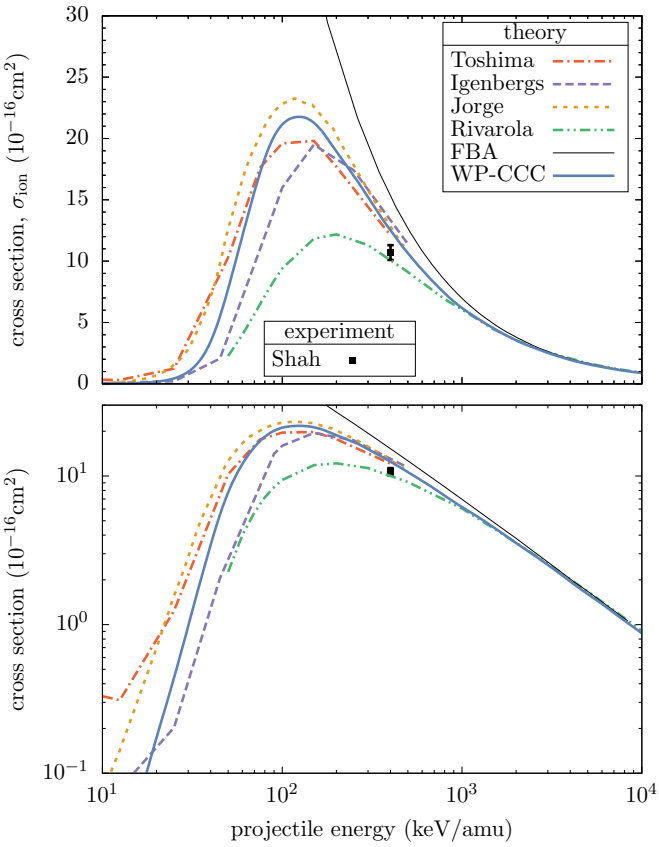

FIG. 5: (color online) The total cross section ($\sigma_{\rm ion}$) for ionization in C^{6+}-H($1s$) collisions: the present WP-CCC results are compared with the experimentally measured point of Shah and Gilbody [6], and the AOCC calculations of Igenbergs et al. [22], Toshima [27], the CTMC calculations of Jorge et al. [23], the CDW-EIS calculations of Rivarola et al. [17], as well as the simple FBA results.

C. Differential ionization cross sections

Genrally speaking, cross sections for differential ionization require inclusion of continuum pseudostates with higher angular momenta than it would be required for obtaining convergent integrated ionization cross sections. That is because in the current approach the ionization amplitude is represented as a decomposition of the vector of the ejected electron momentum in spherical harmonics. Thus, the angular dependence of the ionization amplitude is represented as a sum over the partial terms of this expansion. Therefore, the convergence of these cross sections with respect to $l_{\rm max}$ needs to be studied separately.

In Fig. 6 we present the dependence of the singly differential cross section on the electron ejection angle at different values of the maximum allowed angular momentum of the target and projectile pseudostates for 1 MeV/amu impact ionization. We used denser discretization of the continuum, nevertheless one can see that the convergence of the results with increasing $l_{\rm max}$ is slower than the con-

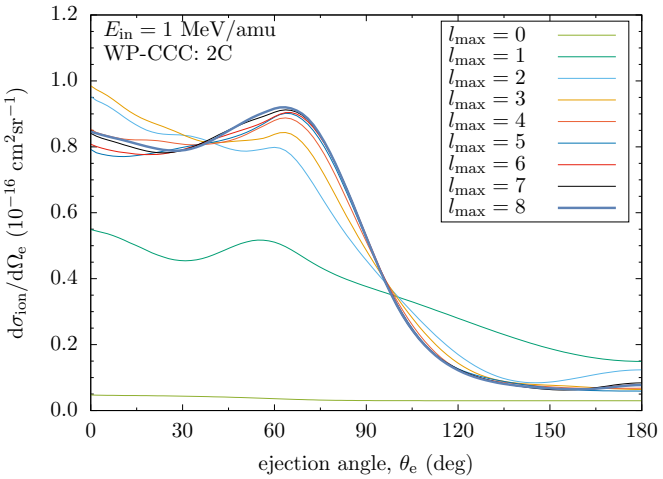

FIG. 6: (color online) The singly differential cross section in the angle of the ejected electron, $d\sigma_{ion}/d\Omega_e$, at 1 MeV/amu impact energy: the convergence of the present two-center WP-CCC results with respect to the maximum included orbital angular momentum quantum number l_{max}.

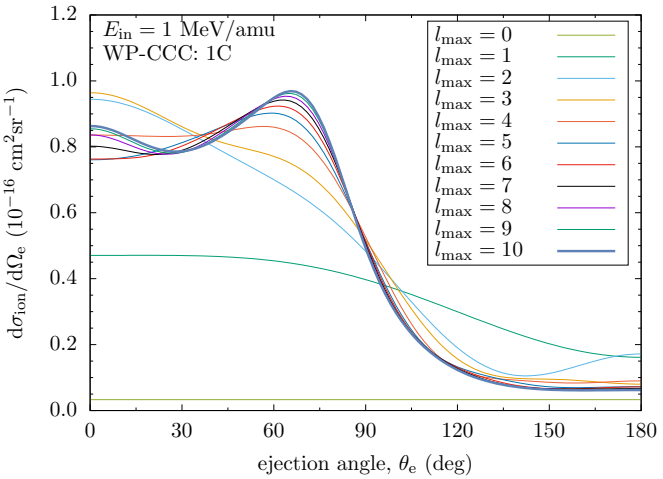

FIG. 7: (color online) The singly differential cross section in the angle of the ejected electron, $d\sigma_{ion}/d\Omega_e$, at 1 MeV/amu impact energy: the convergence of the present one-center WP-CCC results with respect to the maximum included orbital angular momentum quantum number l_{max}.

vergence of the total ionization cross section. Our two-center calculations even with $l_{max} = 8$, which already reach the capacity of the supercomputer available to us, do not produce full convergence still showing slighlty visible variation at small electron ejection angles. Nevertheless,one can see that the SDCS is clearly converging even in the forward direction. Further evidence for it is provided below. In these calculations we utilized $N_b = 10$ bound and $N_c = 30$ positive energy pseudo states on both target and projectile centers. With these basis parameters the size of a two-center basis was altogether 5592 states (2796 on each center).

To verify our two-center calculations and gauge their accuracy we have also done one-center calculations which use only target states. These calculations are significantly simpler and faster though the latter require larger angular momenta to converge. Figures 3 and 5 show that at energies as high as 1 MeV/amu the electron-capture cross section is negligibly smaller than the total ionization cross section. Therefore, the electron loss cross section calculated using the one-center WP-CCC approach should represent the total ionization cross section reasonable well. Thus, the comparison of one-center (1C) and two-center (2C) WP-CCC results can be used to establish the internal consistency of both calculations. Fig. 7 shows the convergence of the one-center WP-CCC results for the same SDCS with respect to l_{max}. Here, we have been able to include the target pseudostates with maximum angular momentum $l_{max} = 10$. As it was the case with two-center calculations the convergence rate is slowest for small electron ejection angles. To explicitly see the convergence pattern at small ejection angles in Fig. 8 we present the l-convergence of the one- and two-center results for this SDCS at the electron ejection angle fixed in the direction of the incident C^{6+} projectile.

As one can see from the figure the two-center results converge faster than the one-center ones. From the displayed convergence pattern one can conclude that the possible remaining error should not exceed a few percent.

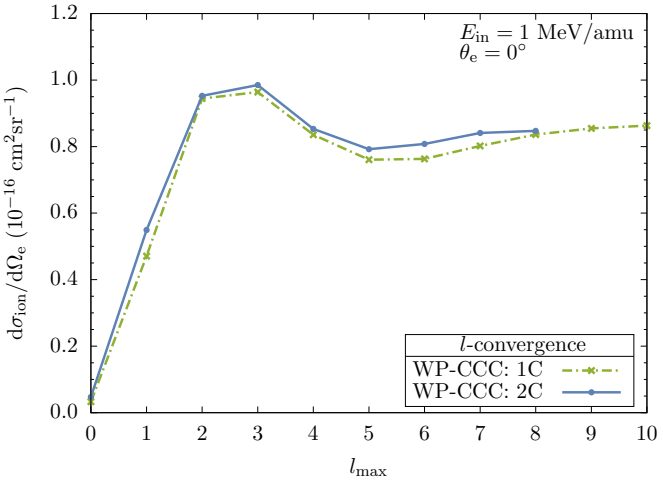

FIG. 8: (color online) The singly differential cross section in the angle of the ejected electron, $d\sigma_{ion}/d\Omega_e$, at 1 MeV/amu impact energy: the convergence of the present one-and two-center WP-CCC results with respect to the maximum included orbital angular momentum quantum number l_{max} at $\theta_e = 0°$ electron ejection angle.

In Fig. 9 our one- and two-center results are compared with the measurements of Tribedi et al. [7, 8] and CDW-EIS calculations. We see that excellent agreement is obtained at all ejected angles except for small ejection angles where the present results overestimate the experimental points. It should be pointed out that both one- and two-center results have a second maximum at 0° ejec-

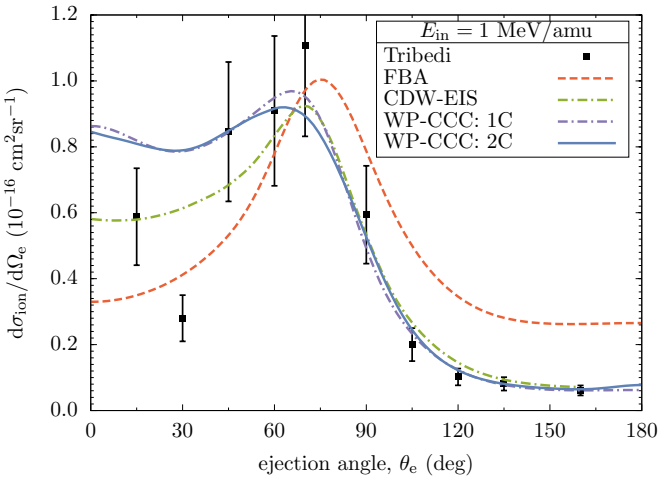

FIG. 9: (color online) The singly differential cross section in the angle of the ejected electron, $d\sigma_{ion}/d\Omega_e$, at 1 MeV/amu impact energy. The measurements and the CDW-EIS calculations of Tribedi et al. [7, 8] and the FBA results are also shown for comparison.

tion angle which is not observed in the FBA and CDW-EIS calculations as well as in the experiment. However, as Tribedi et al. [7] pointed out at the incident angles the measurements were largely affected by a substantial background noise.

The doubly differential cross section (DDCS), $d^2\sigma_{ion}/d\varepsilon d\Omega_e$ are calculated using the two-center basis with maximum allowed angular momentum $l_{max} = 8$ which produced well converged SDCS, $d\sigma_{ion}/d\Omega_e$. It should also be mentioned that the grid for the continuum pseudostate energies was chosen to contain all electron ejection energies considered in the experiment.

Figure 10 shows the dependence of the doubly differential cross section, $d^2\sigma_{ion}/d\varepsilon d\Omega_e$, on the ejected electron energy at 1 MeV/amu impact energy and several electron ejection angles. The comparison is made with the measurements of Tribedi et al. [7, 8], and the CDW-EIS and FBA calculations. For $\theta_e = 15°$ electron ejection angle, the WP-CCC results slightly underestimate the first measured points at 1 and 3 eV, lower than the measurements at 40 and 100 eV, and higher at 200 and 240 eV. For $\theta_e = 45°$, similarly, the current results are lower than the experiment at 1 and 3 eV, but are in very good agreement at all remaining energies. For $\theta_e = 15$ and 45° the FBA results are generally lower than the present results. As we go to higher ejection angle of $\theta_e = 90°$ the agreement with the experiment improves even at 1 and 3 eV. At $\theta_e = 120°$ the WP-CCC results are in line with the experiment everywhere except for the highest ejected energy. For $\theta_e = 90$ and 120° the FBA results are higher than the present results. At all considered ejection angles except for $\theta_e = 90$ the WP-CCC results have some bending at the highest ejected energies. The reason for this feature is the fact that the ECC amplitude peaks around $\boldsymbol{\kappa} \approx \boldsymbol{v}$.

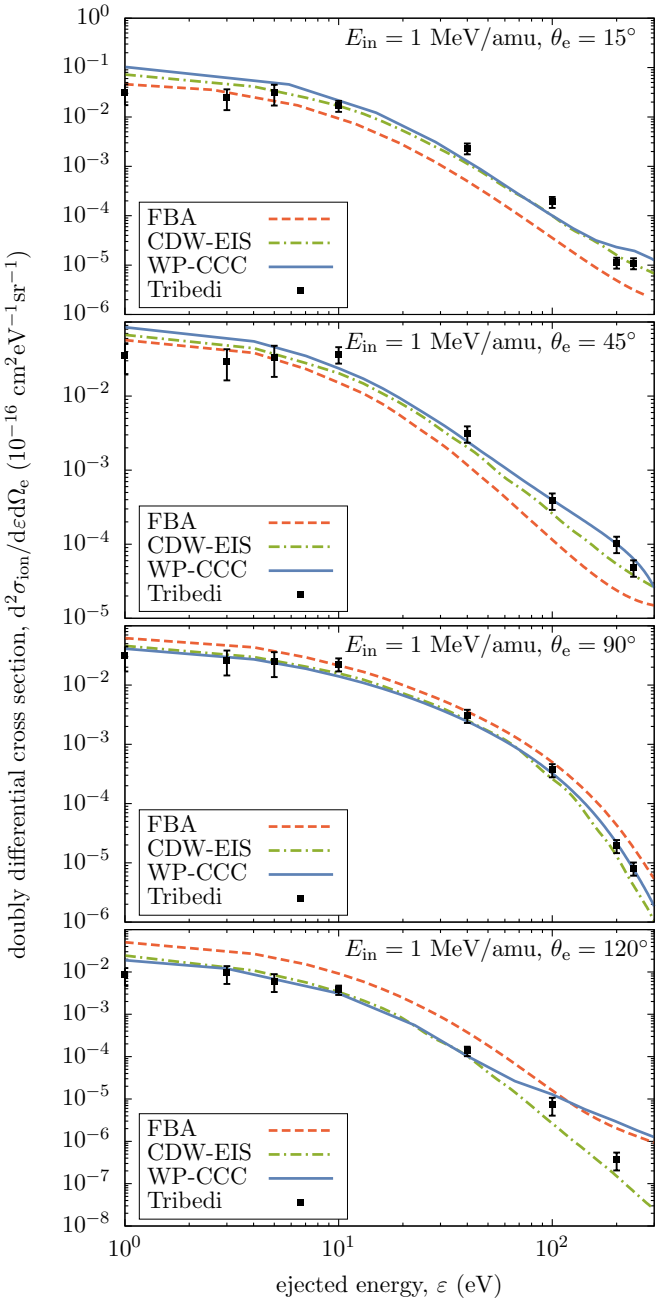

FIG. 10: (color online) The doubly differential cross section in the energy and angle of the ejected electron, $d^2\sigma_{ion}/d\varepsilon d\Omega_e$, at 1 MeV/amu impact energy and indicated electron ejection angles. The measurements and the CDW-EIS calculations of Tribedi et al. [7, 8] and the FBA results are also shown for comparison.

Figure 11 shows the dependence of the doubly differential cross section on the angle of the ejected electron at 1 MeV/amu impact energy and several electron ejection energies. Very good agreement with experiment is obtained at all considered electron ejection energies and angles except for small ejection angles at ejected energies of 3 and 10 eV. Here, our results are higher then exper-

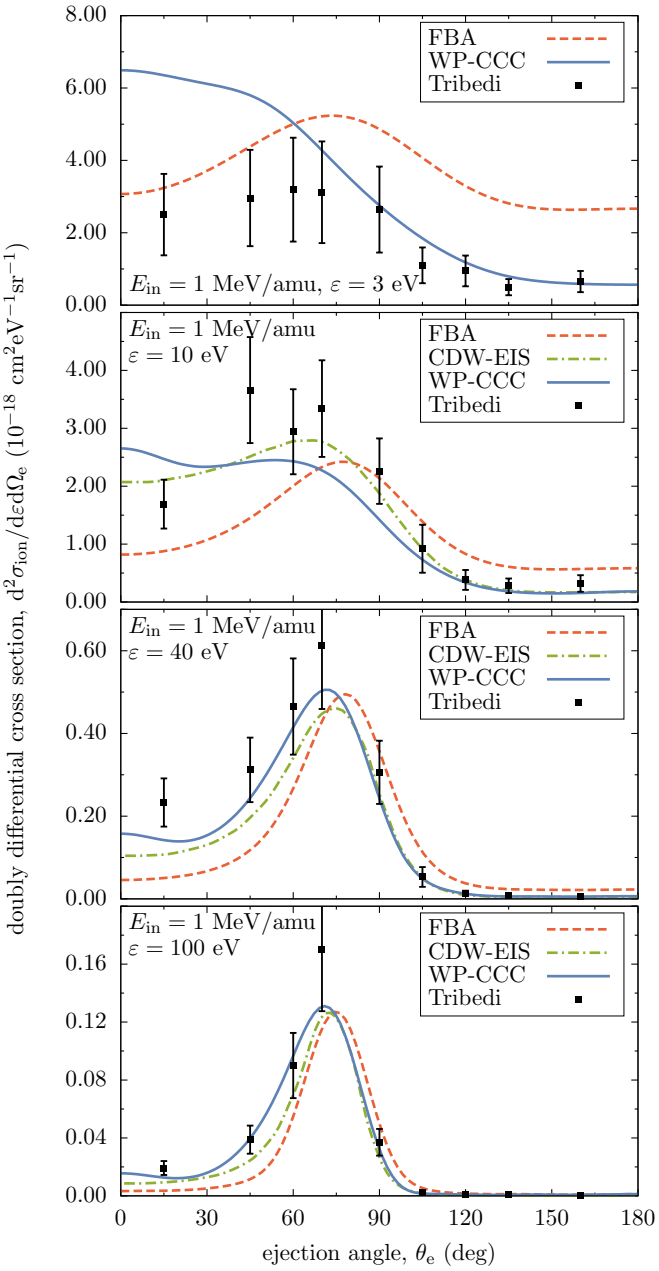

FIG. 11: (color online) The doubly differential cross section in the energy and angle of the ejected electron, $d^2\sigma_{ion}/d\varepsilon d\Omega_e$, at 1 MeV/amu impact energy and indicated electron ejection energies. The measurements and the CDW-EIS calculations of Tribedi et al. [7, 8] and the FBA results are also shown for comparison.

iment and the discrepancy is more pronounced at 3 eV. This in turn leads to disagreement observed near the incident direction in the dependence of the SDCS on the electron ejection angle shown in Fig. 9.

Similar results for the SDCS and DDCS but at 2.5 MeV/amu impact energy are shown in Figs 12-14. With increasing impact energy the convergence of these differential cross sections with respect to the size of the expansion basis becomes even faster. Therefore, the expansion basis employed for 1 MeV/amu impact energy is more than sufficient. At this energy the level of agreement with the experiment is generally better than it is at 1 MeV/amu.

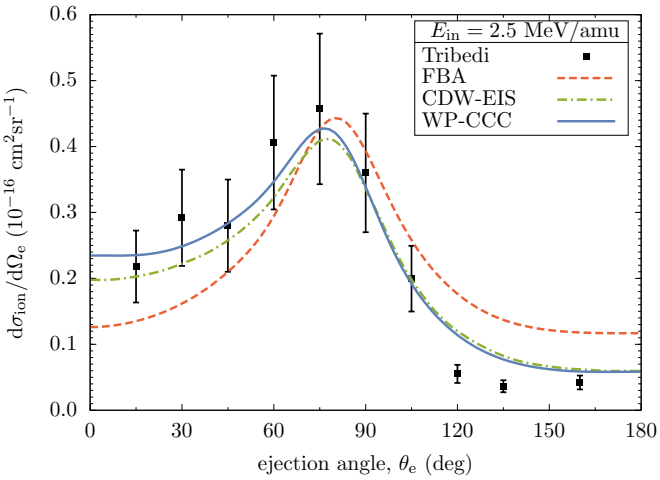

FIG. 12: (color online) The singly differential cross section in the angle of the ejected electron, $d\sigma_{ion}/d\Omega_e$, at 2.5 MeV/amu impact energy. The measurements and the CDW-EIS calculations of Tribedi et al. [7, 8] and the FBA results are also shown for comparison.

The MeV/amu region is considered as easier to deal with, as the energies are high enough for the perturbation approaches to work reasonably well. Although not shown on the graphs for every considered case, at the energies of 1 MeV/amu and 2.5 MeV/amu even the one-center WP-CCC results for the singly and doubly differential ionization, which are somewhat contaminated by the electron-capture cross-section component, are sufficiently accurate and in good agreement with the two-center WP-CCC results. Significantly more challenging is the lower energy region where interplay between all possible reaction channels become important. Figure 15 shows the singly differential cross section in the angle of the ejected electron at 100 keV/amu impact energy. This is a sufficiently low impact energy where the perturbative methods are expected to fail. As one can see from the figure, the present SDCS shows a very different behaviour exhibiting pronounced peak in the forward direction. Note that the FBA predicts a completely unphysical SDCS as a function of the ejected electron angle, where the maximum is observed approximately in the momentum transfer direction. In addition the single-center WP-CCC approach also gives a significantly different result. One can conclude that as collision energy goes down electron capture into the continuum of the projectile strongly enhances electron ejection in the forward direction.

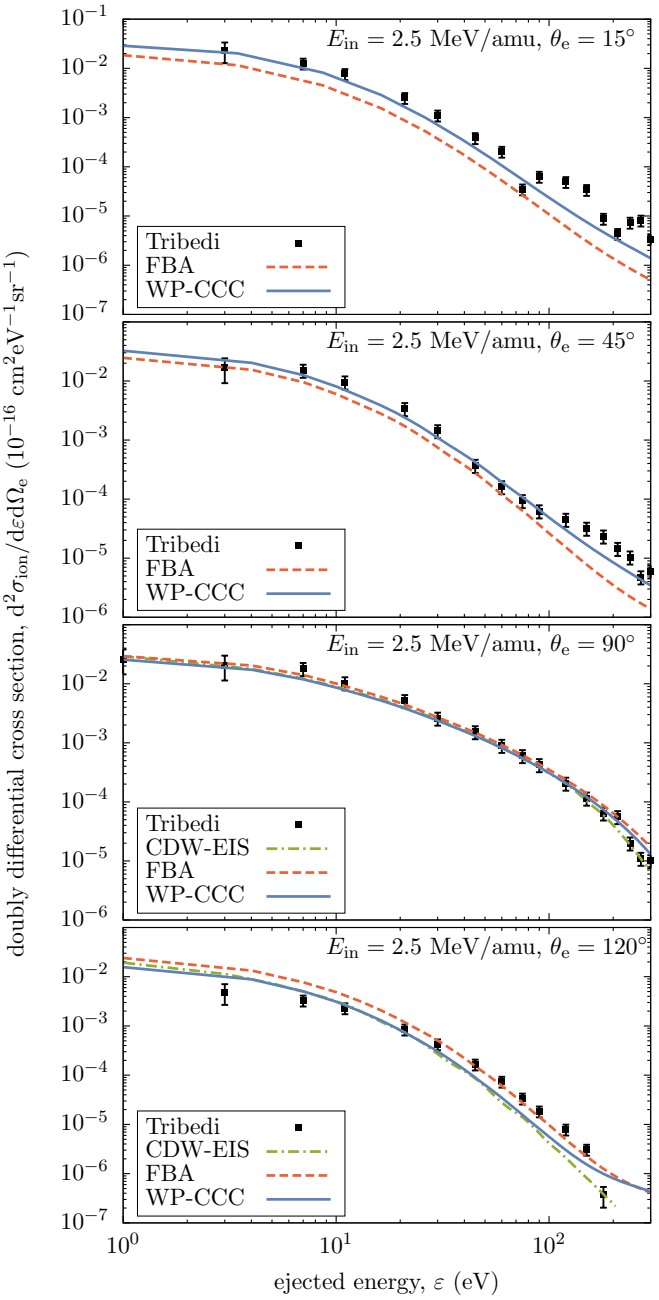

FIG. 13: (color online) The doubly differential cross section in the energy and angle of the ejected electron, $d^2\sigma_{ion}/d\varepsilon d\Omega_e$, at 2.5 MeV/amu impact energy and indicated electron ejection angles. The measurements and the CDW-EIS calculations of Tribedi et al. [7, 8] and the FBA results are also shown for comparison.

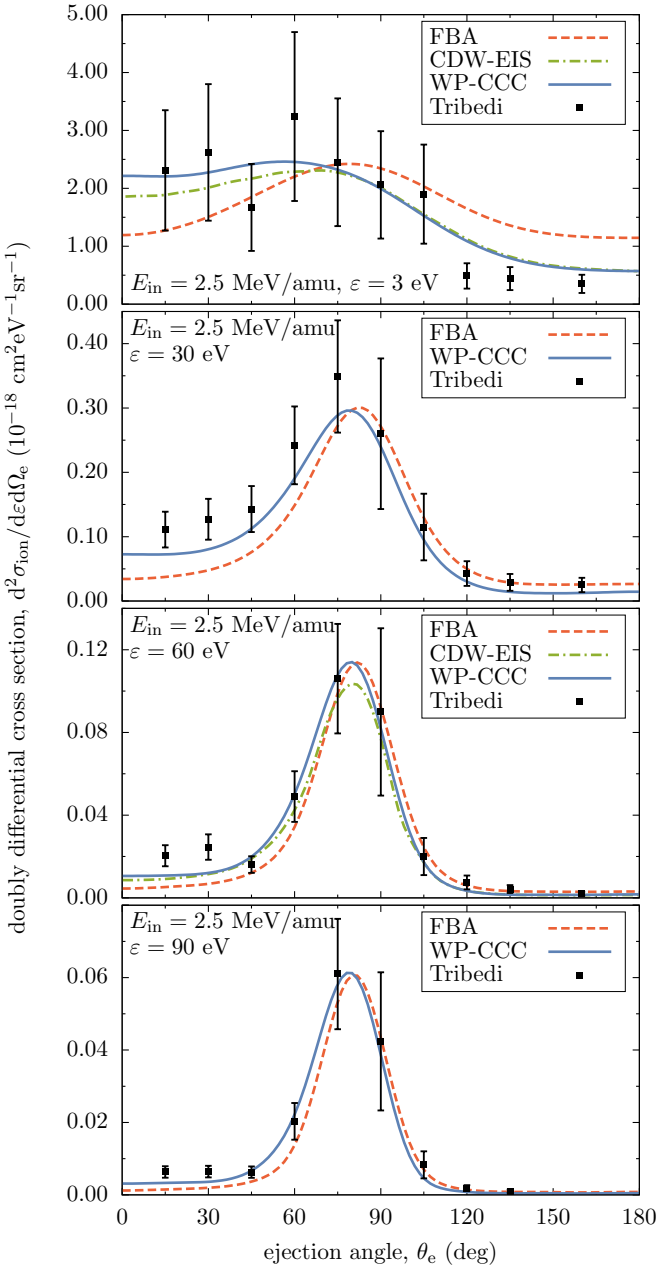

FIG. 14: (color online) The doubly differential cross section in the energy and angle of the ejected electron, $d^2\sigma_{ion}/d\varepsilon d\Omega_e$, at 2.5 MeV/amu impact energy and indicated electron ejection energies. The measurements and the CDW-EIS calculations of Tribedi et al. [7, 8] and the FBA results are also shown for comparison.

IV. CONCLUSIONS

Electron capture and ionization in collisions of bare carbon ions with atomic hydrogen have been studied using the wave-packet continuum discretization approach. The three-body Schrödinger equation governing the collision process is solved using the two-center expansion of the total scattering wavefunction and assuming the projectile motion to be classical. The two-center expansion basis is formed using an orthonormal set constructed from negative-energy eigenstates and wavepacket pseudostates representing the continuum of both the target atom and the atom formed by the projectile after capturing the electron. The usage of wave-packet states allows to discretize continuum arbitrarily which is ideal for dif-

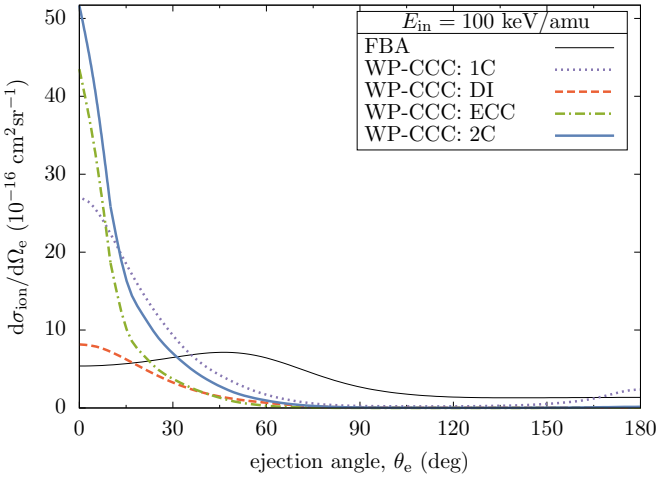

FIG. 15: (color online) The singly differential cross section in the angle of the ejected electron, $d\sigma_{ion}/d\Omega_e$, at 100 keV/amu impact energy. The FBA and one and two-center WP-CCC results are shown for comparison. For two-center WP-CCC results individual DI and ECC contributions are also shown.

ferential ionization studies. In addition, unlike some of the previously employed expansion bases, this basis has full control over the number of included eigenstates as well. This feature is advantageous for largely asymmetric collision systems like the $C^{6+}-H$ one, where the C^{5+} ion formed by the projectile after capturing the electron has a ground-state energy that is 36 times lower than the ground-state energy of atomic hydrogen. Consequently, inclusion of considerably large number of C^{5+} eigenstates is required for convergence. After the expansion of the total scattering wavefunction the Schrödinger equation is converted into coupled-channel first-order differential equations for the transition amplitudes representing elastic scattering, excitation, ionization and electron-capture processes. Calculations have been performed for the projectile energy range from 1 keV/amu to 10 MeV/amu. While there is excellent agreement with experimental data for the total electron-capture cross section over the entire energy range, the calculated total ionization cross section somewhat overestimates the available single measured point. The calculated single and double differential ionization cross sections are in good agreement with experiment at 2.5 MeV/amu. However, at smaller impact energy of 1 MeV/amu there exist considerable discrepancy with experiment at electron ejection angles near the forward direction. Both for SDCS and DDCS the present WP-CCC results exhibit a maximum at these ejection angles which is not observed in the experiment and in the previous theoretical studies. At 100 keV/amu impact energy where the perturbative methods are expected to fail, the present singly differential cross section in the angle of the ejected electron shows very different behaviour. The binary peak in the momentum transfer direction which is characteristic for higher incident energies is replaced with the peak in the forward direction. This peak is significantly more pronounced than it is seen at 1 MeV/amu.

Acknowledgments

This work was supported by the Australian Research Council, the Pawsey Supercomputer Centre, and the National Computing Infrastructure. A.S.K. also acknowledges partial support from the NSF under Grant No. PHY-1415656.

[1] O. Marchuk, Phys. Scr. **89**, 114010 (2014), URL http://stacks.iop.org/1402-4896/89/i=11/a=114010.
[2] O. Marchuk, Y. Ralchenko, and D. R. Schultz, Plasma Phys. Control. Fusion **54**, 095010 (2012), URL http://stacks.iop.org/0741-3335/54/i=9/a=095010.
[3] D. Belkić, J. Math. Chem. **47**, 1366 (2010).
[4] F. W. Meyer, A. M. Howald, C. C. Havener, and R. A. Phaneuf, Phys. Rev. A **32**, 3310 (1985), URL https://link.aps.org/doi/10.1103/PhysRevA.32.3310.
[5] T. V. Goffe, M. B. Shah, and H. B. Gilbody, Journal of Physics B: Atomic and Molecular Physics **12**, 3763 (1979), URL http://stacks.iop.org/0022-3700/12/i=22/a=021.
[6] M. B. Shah and H. B. Gilbody, Journal of Physics B: Atomic and Molecular Physics **16**, L449 (1983), URL http://stacks.iop.org/0022-3700/16/i=15/a=005.
[7] L. C. Tribedi, P. Richard, W. DeHaven, L. Gulys, M. W. Gealy, and M. E. Rudd, Journal of Physics B: Atomic, Molecular and Optical Physics **31**, L369 (1998), URL http://stacks.iop.org/0953-4075/31/i=8/a=007.
[8] L. C. Tribedi, P. Richard, L. Gulys, and M. E. Rudd, Physica Scripta **1999**, 333 (1999), URL http://stacks.iop.org/1402-4896/1999/i=T80B/a=068.
[9] L. C. Tribedi, P. Richard, L. Gulyás, M. E. Rudd, and R. Moshammer, Phys. Rev. A **63**, 062723 (2001), URL https://link.aps.org/doi/10.1103/PhysRevA.63.062723.
[10] J. R. Oppenheimer, Phys. Rev. **31**, 349 (1928).
[11] H. C. Brinkman and H. A. Kramers, Proc. Acad. Sci. Amsterdam **33**, 973 (1930).
[12] J. D. Jackson and H. Schiff, Phys. Rev. **89**, 359 (1953).
[13] B. H. Bransden and M. R. C. McDowell, *Charge Exchange and the Theory of Ion-Atom Collisions* (Clarendon, Oxford, 1992).
[14] D. Belkic, S. Saini, and H. S. Taylor, Phys. Rev. A **36**, 1601 (1987).
[15] D. Belkic, R. Gayet, and A. Salin, Phys. Rep. **56**, 279 (1979).
[16] D. S. F. Crothers and J. F. McCain, J. Phys. B **16**, 3229 (1983).
[17] R. D. Rivarola, P. D. Fainstein, and V. H. Ponce, Physica Scripta **1989**, 101 (1989), URL http://stacks.iop.

org/1402-4896/1989/i=T28/a=018.
[18] R. E. Olson and A. Salop, Phys. Rev. A **16**, 531 (1977).
[19] D. J. W. Hardie and R. E. Olson, Journal of Physics B: Atomic and Molecular Physics **16**, 1983 (1983), URL http://stacks.iop.org/0022-3700/16/i=11/a=018.
[20] R. E. Olson and D. R. Schultz, Physica Scripta **1989**, 71 (1989), URL http://stacks.iop.org/1402-4896/1989/i=T28/a=013.
[21] J. Fiol and R. E. Olson, Journal of Physics B: Atomic, Molecular and Optical Physics **35**, 1759 (2002), URL http://stacks.iop.org/0953-4075/35/i=7/a=312.
[22] K. Igenbergs, J. Schweinzer, A. Veiter, L. Perneczky, E. Frhwirth, M. Wallerberger, R. E. Olson, and F. Aumayr, Journal of Physics B: Atomic, Molecular and Optical Physics **45**, 065203 (2012), URL http://stacks.iop.org/0953-4075/45/i=6/a=065203.
[23] A. Jorge, L. F. Errea, C. Illescas, and L. Méndez, Eur. Phys. J. D **68**, 227 (2014), URL https://doi.org/10.1140/epjd/e2014-50109-4.
[24] C. Harel, H. Jouin, and B. Pons, Atomic Data and Nuclear Data Tables **68**, 279 (1998), ISSN 0092-640X, URL http://www.sciencedirect.com/science/article/pii/S0092640X97907683.
[25] M. Kimura and C. D. Lin, Phys. Rev. A **32**, 1357 (1985), URL https://link.aps.org/doi/10.1103/PhysRevA.32.1357.
[26] T. A. Green, E. J. Shipsey, and J. C. Browne, Phys. Rev. A **25**, 1364 (1982), URL https://link.aps.org/doi/10.1103/PhysRevA.25.1364.
[27] N. Toshima, Phys. Rev. A **50**, 3940 (1994).
[28] N. Toshima, Phys. Rev. A **50**, 3940 (1994), URL https://link.aps.org/doi/10.1103/PhysRevA.50.3940.
[29] I. B. Abdurakhmanov, J. J. Bailey, A. S. Kadyrov, and I. Bray, Phys. Rev. A **97**, 032707 (2018), URL https://link.aps.org/doi/10.1103/PhysRevA.97.032707.
[30] S. Chandrasekaran and G. Juckeland, *OpenACC for Programmers: Concepts and Strategies* (Addison-Wesley Professional, 2017).
[31] I. B. Abdurakhmanov, S. U. Alladustov, J. J. Bailey, A. S. Kadyrov, and I. Bray, Plasma Physics and Controlled Fusion **60**, 095009 (2018).
[32] I. B. Abdurakhmanov, A. S. Kadyrov, I. Bray, and K. Bartschat, Phys. Rev. A **96**, 022702 (2017), URL https://link.aps.org/doi/10.1103/PhysRevA.96.022702.
[33] S. K. Avazbaev, A. S. Kadyrov, I. B. Abdurakhmanov, D. V. Fursa, and I. Bray, Phys. Rev. A **93**, 022710 (2016).
[34] I. B. Abdurakhmanov, A. S. Kadyrov, S. K. Avazbaev, and I. Bray, J. Phys. B **49**, 115203 (2016).
[35] *CuSolver Library* (NVIDIA Corporation, 2018).
[36] D. R. Bates, Proc. Roy. Soc. A **247**, 294 (1958).
[37] Comparative study of the coherent and incoherent combinations of the components was performed in [29] in the example of p-H ionization. For all practical purposes the incoherent combination, which is computationally less demanding, was shown to be an acceptable proposition.